

Automated identification of current sheets – a new tool to study turbulence and intermittency in the solar wind

Olga Khabarova^{1,2}, Timothy Sagitov³, Roman Kislov^{1,2}, and Gang Li⁴

¹Pushkov Institute of Terrestrial Magnetism, Ionosphere and Radiowave Propagation of the Russian Academy of Sciences (IZMIRAN), Troitsk, Moscow 108840, Russia;
habarova@izmiran.ru .

²Space Research Institute of the Russian Academy of Sciences (IKI), Moscow 117997, Russia.

³Higher School of Economics University (HSE), Moscow 101000, Russia

⁴Center for Space Plasma and Aeronomics Research (CSPAR), University of Alabama in Huntsville, Huntsville, AL 35805, USA.

Corresponding author: Olga Khabarova (habarova@izmiran.ru)

Key Points:

- We propose a new method of the automated identification of current sheets based on a technique commonly used by observers.
- A multiyear list of current sheets identified at 1 AU is available at <https://csdb.izmiran.ru>
- The number of CSs per day (R) is determined by variations of the kinetic and thermal energy density of the solar wind.

Abstract

We propose a new method of the automated identification of current sheets (CSs) that represents a formalization of the visual inspection approach employed in case studies. CSs are often identified by eye via the analysis of characteristic changes in the interplanetary magnetic field (IMF) and plasma parameters. Known visual and semi-automated empirical methods of CS identification are exact but do not allow a comprehensive statistical analysis of CS properties. Existing automated methods partially solve this problem. Meanwhile, these methods suggest an analysis of variations of the IMF and its direction only, being based on Taylor’s hypothesis applicable mainly to turbulent plasmas but not to CSs of all kinds. In our three-parameter empirical method, we employ both the solar wind plasma and IMF parameters to identify CSs of various types. Derivatives of the IMF strength, the plasma beta and the ratio of the Alfvén speed V_A to the solar wind speed V taken with the one-second cadence are used. We find that the CS daily rate R correlates with the solar wind temperature T rather than with V and is proportional to the sum of the kinetic and thermal energy density $\sim V^2(N+5N') + 10T(N+N')$, where $N' = 2\text{cm}^{-3}$ is the background level of the solar wind density N . Maxima of R are associated with stream/corotating interaction regions and interplanetary mass ejection sheaths. A multiyear list of CSs identified at 1 AU can be found at <https://csdb.izmiran.ru>.

Plain Language Summary

We formalize an experience of observers in identifying current sheets (CS) via the analysis of typical changes in the interplanetary magnetic field and solar wind plasma parameters. A new automated method of CS identification is created, and an open access multi-year database of CSs observed at 1 AU is compiled. We find that the daily rate of CSs is determined by variations of the kinetic and thermal energy density of the solar wind.

1 Introduction

Current sheets (CSs) in the solar wind are specific discontinuities carrying the electric current that contributes to the global electric circuit of the heliosphere (Wilcox & Ness 1965, Svalgaard et al., 1983; Suess et al., 2009; Kislov et al., 2015, 2019; Maiiewski et al., 2020). On the one hand, these structures may be formed as a result of turbulence and various dynamical processes occurring in the solar wind, and, on the other hand, some of CSs are of the solar origin. One of the most important features known about CSs is that, independently of their origin, their width is approximately the same (\sim several proton gyroradii), while their elongation varies considerably depending on the way of their formation (Malova et al., 2017). The CSs that represent elongated neutral lines of the solar magnetic field are the most stable structures that may extend to the outer heliosphere, and, in turn, the turbulence-born CSs are much shorter, very dynamic and unstable by nature (Li, 2008; Zhdankin et al., 2013; Podesta, 2017; Zelenyi et al., 2020).

The last decade brought a lot of discoveries about properties of CSs in space plasmas, mainly owing to the fast development of the numerical analysis methods such as magnetohydrodynamic numerical simulations of fluids that allow studying CS formation in turbulent plasmas (e.g., www.mhd turbulence.com; Burkhardt et al., 2020), the Test Particle (TP) and Particle-In-Cell (PIC) coding on supercomputers (e.g., Hesse et al., 2001; Pritchett, 2003; Muñoz & Büchner 2018; Xia & Zharkova, 2018, 2020), and so-called General-Purpose

computing on Graphics Processing Units (GPGPU) (e.g., <https://gyires.inf.unideb.hu/KMITT/a53/ch05.html>; Dokken et al., 2007; Mingalev et al., 2019, 2020).

Recent advances in case studies of CSs in the solar wind have also contributed to better understanding of the CS fine structure and processes associated with CS dynamics. Overall, there were confirmed (i) 3-D stochastic nature of CSs, (ii) self-organization of CSs, (iii) their multi-layered fine structure, (iv) a strong connection between CSs and magnetic islands/plasmoids, and (v) their important role in particle acceleration in space plasmas (e.g., Khabarova et al., 2015, 2016; Khabarova & Zank, 2017; le Roux et al. 2019; Adhikari et al., 2019; Malandraki et al., 2019; Lazarian et al. 2020; Tan, 2020).

In contrast to case studies and simulations, statistical studies of CSs are infrequent in this area (e.g., Li, 2008; Zhang et al., 2008; Suess et al., 2009; Borovsky & Denton, 2011; Li et al., 2011; Malova et al., 2017; Podesta, 2017), and, obviously, a lot of information is still missed because of the lack of a comprehensive statistical analysis. The absence of an easily accessible database of CSs subsequently identified for a prolonged period lays researches under a necessity to compile their own short CS lists coming from case studies (e.g., Suess et al., 2009; Malova et al., 2017; Burkholder & Otto, 2019; Borovsky & Burkholder, 2020; http://www.srl.caltech.edu/ACE/ASC/DATA/level3/swepam/ACE_ExhaustList.pdf; <https://lasp.colorado.edu/mms/sdc/public/about/events/#/>).

Such lists typically consist of tens-hundreds CSs or reconnection exhaust crossings randomly picked for months or even years, while the rate of the occurrence of CSs is \sim hundreds CSs per hour (see Li (2008), Podesta (2017), and results of this study). Therefore, a problem of the insufficient progress in CS studies is that the manual identification of CSs remains the most frequently used way to analyze CS properties. A significant loss of information under such an approach is obvious.

To solve the problem, methods of the CS identification that suggest some automatization have been proposed. An automated method of identification of discontinuities of various types can be used first, - for example, a Partial Variance of Increments (PVI) method (Greco et al., 2009, 2018) that identifies all discontinuities, including shocks, or a method of the identification of magnetic holes carrying current sheets at their borders (Winterhalter et al., 1994; Zhang et al., 2008). If the identification of coherent structures is subsequently complemented by a visual inspection, this allows extracting of CSs from the whole body of events (e.g., Zhang et al., 2008; Malandraki et al., 2019). Such methods are called semi-automated.

There are fully automated methods allowing the CS identification (Li, 2008; Zhdankin et al., 2013; Podesta, 2017; Azizabadi et al., 2020; Pecora et al., 2021). The most popular among them are Gang Li's method (Li, 2008) and John Podesta's method (Podesta, 2017). Gang Li's method is based on the analysis of the IMF angle variations, supposing that a CS crossing is always accompanied by a sharp change in the local magnetic field direction (Li, 2008; Li et al., 2011; Miao et al., 2011). The method works well in turbulent plasmas. The current density calculation is the other way to find a CS location (Podesta, 2017). To calculate the necessary derivatives, one should perform a transition from time dependences $\mathbf{B}(t)$ to spatial $\mathbf{B}(\mathbf{r})$. When studying CSs associated with turbulence, Taylor's hypothesis is usually employed, according to which disturbances propagate together with the plasma flow, i.e. $d\mathbf{B}/dt - V_{SW}d\mathbf{B}/dr = 0$, where V_{SW} is the solar wind speed, \mathbf{B} is the magnetic field vector, and r is the coordinate along the of the solar wind speed direction (see Podesta, 2017 for detailed explanations). Using Taylor's hypothesis, one can identify CSs embedded in specific flows and consisting of particles that

move with the structure. Within this approach, all automated methods cited above can successfully be applied to the turbulent solar wind.

Meanwhile, some CSs are associated with plasma structures which propagate with the speed different from the surrounding solar wind speed, i.e. such current-carrying structures are not embedded in the feely expanding solar wind and consist of different particles all the time. This is the case of quasi-stationary CSs formed (i) at shocks and strong discontinuities, including the heliospheric current sheet (HCS) and other CSs of the solar origin, the terrestrial magnetopause, leading edges of interplanetary coronal mass ejections (ICMEs), and fast flows from coronal holes, and (ii) owing to interactions of wave fronts (Wilcox & Ness, 1965; Svalgaard et al., 1983; Dunlop et al., 2002; Khabarova et al., 2015, 2016, 2017a, b, 2018; Khabarova & Zank, 2017; Le Roux et al. 2019; Malandraki et al., 2019). If a spacecraft crosses such a structure, an attempt to calculate the electric current density according to Taylor's hypothesis may lead to an error, and the obtained electric current may have an incorrect magnitude and direction. Furthermore, the larger-scale CSs of the non-turbulent origin may create or be surrounded by other structures, namely, secondary CSs and magnetic islands that cannot formally be attributed to turbulence either but is treated as intermittent structures in case studies (e.g., Khabarova et al., 2015, Adhikari et al., 2019). A notable example is the heliospheric plasma sheet (HPS) surrounding the HCS (Winterhalter et al., 1994; Simunac et al., 2012). Multiple structures observed within the HPS represent both CSs originated from the extension of coronal streamers and locally-born coherent structures, namely, CSs and magnetic islands (Khabarova & Zastenker, 2011; Khabarova et al., 2015, 2017b, 2018; Maiewski et al., 2020).

Therefore, it makes sense to enhance a CS identification based on variations of the magnetic field by considering additional plasma features widely used by specialists to find CSs by eye (Suess et al., 2009; Khabarova et al., 2015, 2016, 2017b, 2018, 2020; Khabarova & Zank 2017; Malova et al., 2017; Adhikari et al., 2019). In this work, we formalize the experience of observers in visual inspection of typical changes of the IMF and the solar wind plasma parameters at CS crossings, turning it into a new automated method of CS identification. A multi-year list of CSs observed at 1 AU is compiled as a result of this study.

2 Data and Method

2.1 Data

Our study is mainly based on an analysis of the Advanced Composition Explorer (ACE) measurements. ACE is one of the key 1 AU spacecraft located between the Earth and the Sun at the 1st Lagrange point (see <http://www.srl.caltech.edu/ACE/>, Stone et al., 1998). We have used the following ACE data for 2004-2010: the IMF magnitude B measured with the one second resolution and the 64-second-resolution plasma data, namely, the solar wind proton number density N , the solar wind bulk speed V , and the radial component of the proton temperature T (<https://cdaweb.gsfc.nasa.gov/>)

The other dataset employed is from the STEREO Ahead (A) and STEREO Behind (B) spacecraft that move nearly along the Earth's orbit in the opposite direction with respect to each other (see <https://stereo-ssc.nascom.nasa.gov/data.shtml> and Kaiser et al., 2008). STEREO A is a little closer to the Sun, and STEREO B is a little further from the Sun than the Earth (<https://stereo-ssc.nascom.nasa.gov/where.shtml>). The STEREO mission data on B with the one

second resolution https://stereo-dev.epss.ucla.edu/l1_data, and the plasma parameters (N , V and T) with the 60 second resolution are obtained from <https://cdaweb.gsfc.nasa.gov/>. Currently, only STEREO A remains operating, but we use the STEREO A and STEREO B data for several-day-long intervals taken in 2007-2010 when both spacecraft functioned normally. The STEREO data are not used in the compiling of our open-access CS list.

The plasma data have been interpolated and calculated with the one-second span that allows us to compute the plasma beta β (the ratio of the plasma pressure to the magnetic pressure) and the Alfvén speed V_A with the span corresponding to the IMF resolution (see the parameter derivation technique at https://omniweb.gsfc.nasa.gov/ftpbrowser/bow_derivation.html). At the next step, the one-second derivatives of B , β , and V_A/V are calculated to identify CSs (see the Method).

In order to trace CSs observed within specific flows, we identify SIRs first from 3-D reconstructed pictures of the normalized density in the ecliptic plane obtained from the Heliospheric Imager (HI) instruments on board of the STEREO spacecraft (<http://helioweb.net>). Using HIs is a unique way to look at the dynamic picture of the behavior of streams/flows in the interplanetary medium. One can find key information about HI observations in white light, the techniques allowing the solar wind density reconstruction from the observations, and the related studies in the following articles: Bisi et al. (2008); Eyles et al. (2008, 2009); Rouillard et al. (2008); Jackson et al. (2009); Scott et al. (2019); Barnard et al. (2020).

Finally, a CS database for ACE compiled by Gang Li according to his method of the automated CS identification (Li, 2008) has been compared with the database resulted from our study (<https://csdb.izmiran.ru>).

2.2 Method

We suggest a formalization of the long-time experience of observers in the visual identification of CSs based on the analysis of the IMF and plasma parameters that vary sharply at CSs of different origins in the solar wind (Behannon et al., 1981; Blanco et al., 2006; Zhang et al., 2008; Suess et al., 2009; Simunac et al., 2012; Zharkova & Khabarova, 2012, 2015; Khabarova et al., 2015, 2016; Khabarova & Zank 2017; Malova et al. 2017; Adhikari et al., 2019). As an example, a characteristic crossing of a CS detected by the Wind spacecraft at 1 AU on 25 June 2004 is shown in Figure 1 (adapted from Khabarova et al., 2020). The IMF magnitude B sharply decreases because of the neutral line crossing. The horizontal B_x IMF component in the GSE coordinate system passes through zero. Generally, a CS crossing is characterized by a sign reverse of at least one of the IMF components. Consequently, the azimuthal IMF angle B_{phi} sharply varies, indicating the IMF vector direction change to the opposite. Both the solar wind density and the plasma beta increase at the CS. V and T may slightly increase at CSs, owing to ongoing magnetic reconnection (Gosling et al., 2005; Adhikari et al., 2019; Phan et al., 2020). The solar wind speed change itself is usually too weak and cannot be used for the CS identification. Meanwhile, the V_A/V ratio decrease observed under both a high and low resolution at CSs is substantial and may be considered as an important key to recognize CSs (Suess et al., 2009).

It should be noted that although CSs are crossed for seconds, their crossings are seen differently under different time/space resolutions. A strong CS crossing (the HCS, for example) considered with the hourly and even daily resolution is associated with an increase in B encompassing the CS occurrence hour/day (Khabarova & Zastenker, 2011), while under at least

a minute resolution it is seen as a decrease in B . This phenomenon is explained by the occurrence of dynamical processes at CSs that change properties of plasma surrounding CSs (see Zharkova & Khabarova, 2012, 2015; Zelenyi et al., 2016; Malova et al., 2017, 2018 and references therein).

Therefore, the main features seen with a resolution not worse than one minute that may characterize a CS crossing are following: (i) a decrease in B , (ii) a decrease in V_A/V , and (iii) an increase in β . It is easy to find that all other peculiarities are linked with the listed ones. Since the automatization of the CS recognition process requires setting the same rules for CSs occurring in different plasmas under different conditions, normalization should be performed. Hence, after obtaining B , V_A/V , and β , we calculate their one-second derivatives. One can suggest then that spikes of the derivatives reflect the location of CSs.

Noise cutoff or a threshold choice is the most sensitive point of new methods. Its introduction is always based on the experience and common sense. We have chosen to carefully compare the results with clear cases of CS crossings discussed in literature and find the optimal

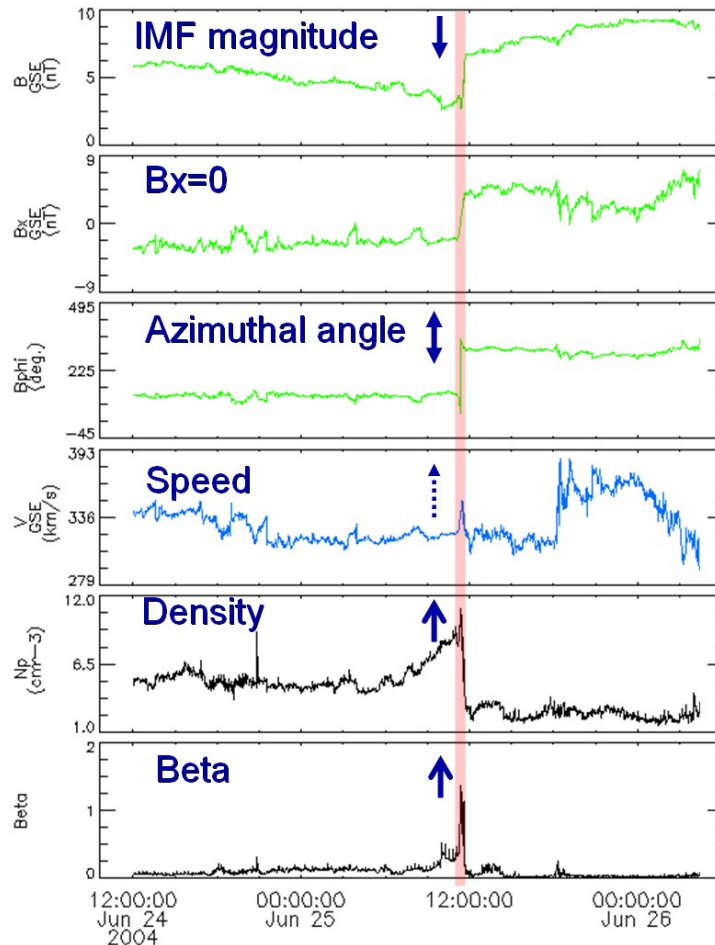


Figure 1. Typical behavior of the IMF and plasma parameters at a CS crossing. From top to bottom: the IMF magnitude, the horizontal IMF component B_x , the IMF azimuthal angle B_{ϕ} , the solar wind speed V and density N_p , and the plasma beta. Wind spacecraft one-minute resolution data are used. CS crossing and the associated changes in the IMF and plasma parameters are depicted by the pink stripe and arrows. Event analyzed by Zharkova & Khabarova (2012).

parameter levels above which the peaks correspond to the CS location in the best way. The first threshold of $\beta=3$ for a one second resolution data has been imposed. The next important point is that the signatures of a CS crossing discussed above should be considered altogether. In statistical terms this means finding a maximum correlation between different datasets to restrict final results by those complying with necessary signatures observed in all key parameters.

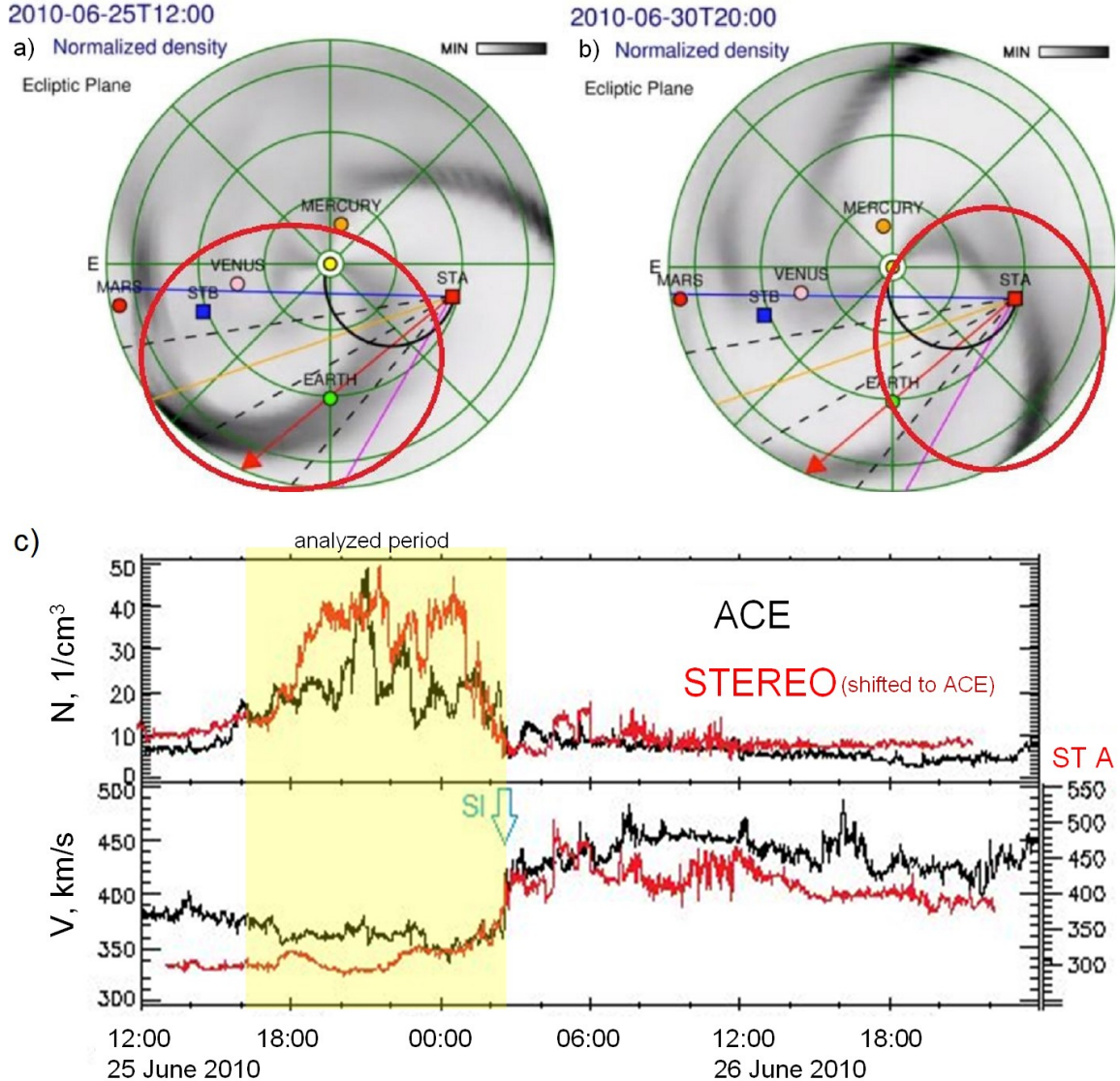


Figure 2. SIR subsequently observed by ACE and STEREO on 25-30 June 2010. a) Normalized plasma density shown in the ecliptic plane is reconstructed from the HI observations on board of STEREO. Earth – the green dot; the Sun is the yellow dot in the center. Red circles encompass the SIR of interest. SIR passes the Earth. b) the same but the SIR reaches STEREO A. Corresponding movie can be seen at <http://heliowebster.net/archive/2010/06/sta1dej.html>. c) In situ observations of the solar wind density N and speed V by ACE (black) and STEREO A (red). STEREO A data are shifted to ACE.

Applying the maximum correlation condition, we finally obtain the following thresholds: values above $dB/dt = -0.14$, below $d\beta/dt = 0.11$, and above $d(V_A/V)/dt = -0.003$ are considered as noise; here $t = 1$ s. Note that the thresholds will be different if one considers a lower resolution or averaged data. We treat variations in dB/dt as the main feature, therefore only the spikes that appear simultaneously in dB/dt and any of two other parameters are considered as pointing out the CS location.

These are the key points on which a new method of the automated identification of CSs is based. Details are illustrated below step by step in the process of identification of CSs embedded in a stream interaction region (SIR).

3 Identification of CSs – results

3.1 Illustration of finding CSs from the ACE and STEREO data

To demonstrate how the method works, we apply the technique to a SIR, the region not

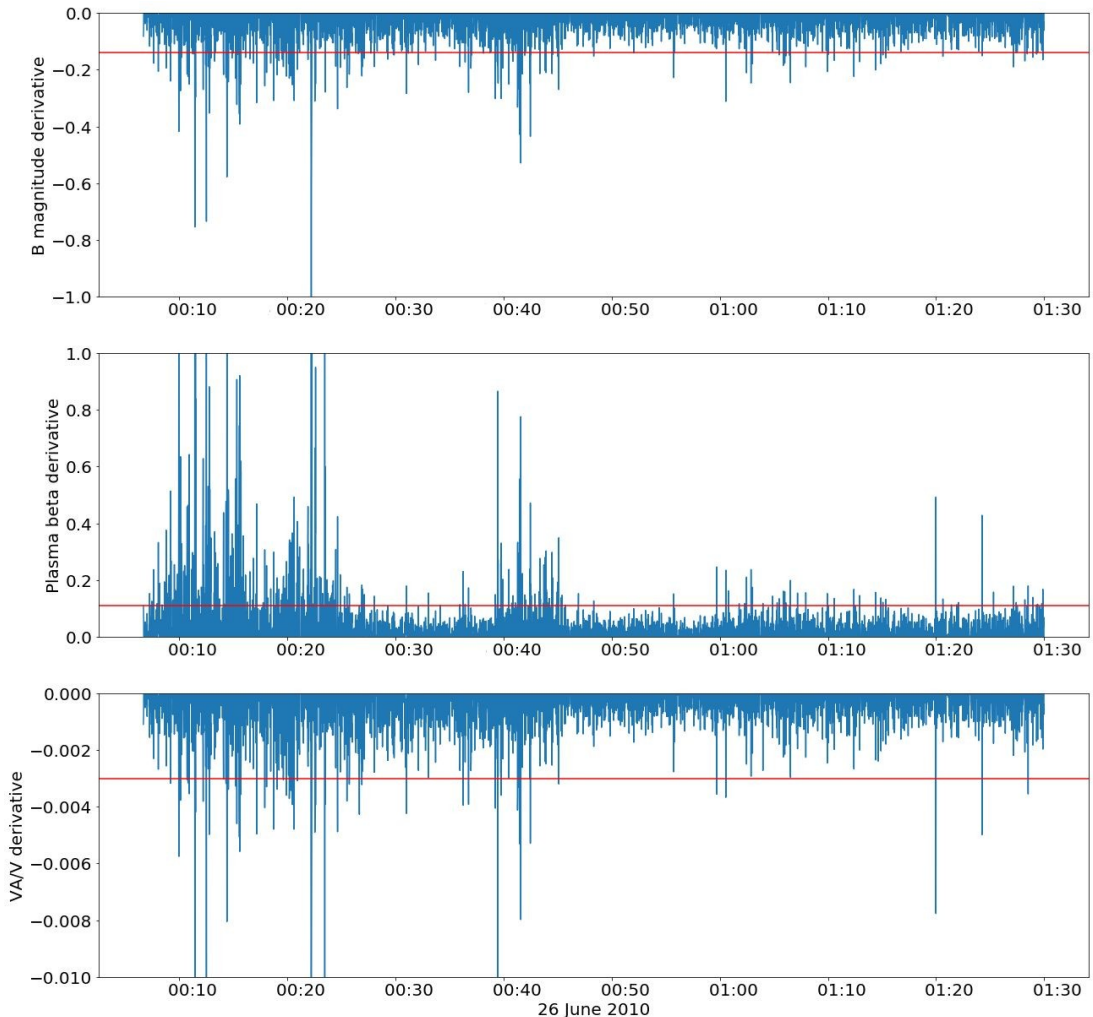


Figure 3. Example of automated identification of CSs via the three-parameter method. Based on the analysis of the ACE data, one second cadence. From top to bottom: derivatives of B , β , and V_A/V . Red lines indicate the noise cut off level (see 2.2. Method). Spikes indicate the CS location. Database of CSs identified at 1 AU is provided at <https://csdb.izmiran.ru> .

freely propagating in the solar wind but resulting from the interaction of a rotating high-speed flow from a coronal hole with the ambient slower solar wind. A SIR resembles an ICME sheath by properties since it is equally turbulent and full of numerous discontinuities, CSs and magnetic islands (e.g., Ho et al., 1996; Jain et al., 2006; Tassein et al., 2011; Khabarova et al., 2017b). A description of key features of SIRs and their long-lived counterparts, corotating interaction regions (CIRs), can be found in a comprehensive review by Ian Richardson (see Richardson, 2018 and references therein).

SIRs are important drivers of space weather living in the interplanetary medium much longer than ICMEs that quickly expand, pass 1 AU in 1-3 days and fade with distance. Since SIRs linked to coronal hole flows, they rotate for many days, striking planets and spacecraft one by one, which gives us an opportunity to study these large-scale structures as a whole and in detail. SIRs/CIRs can be traced remotely via HIs designed to observe dynamics of dense solar wind structures in white light (see 2.1 Data). Such a tracking is necessary (i) to be sure that two different spacecraft detect the same flow (if one analyzes *in situ* measurements), (ii) to be confident that the flow is not interrupted by an ICME for time enough to observe it *in situ*, (iii) to compute the angular speed of the rotating flow, and, finally, (iv) to analyze a longitudinal evolution of SIRs/CIRs.

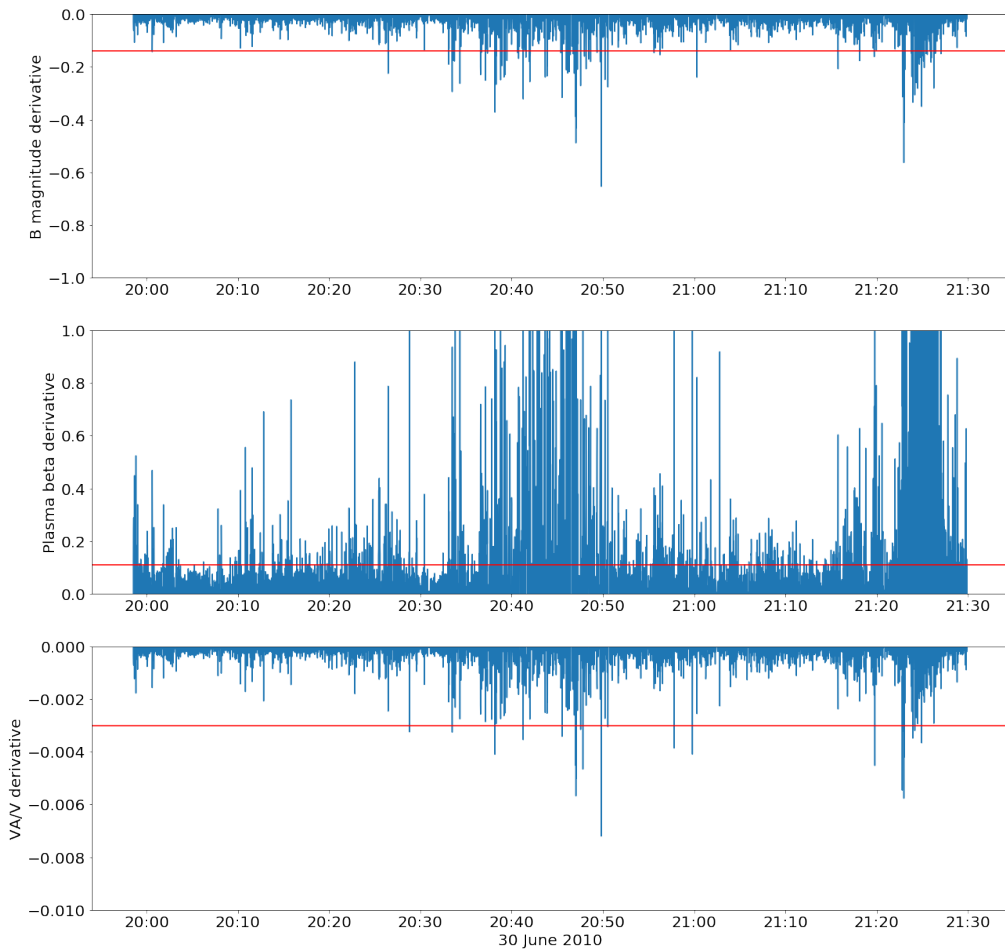


Figure 4. Analogous to Figure 3, but for STEREO A data, one second cadence.

Figure 2 is an example of the analysis of the SIR evolution using both the STEREO HI abilities and in situ measurements. Figure 2b shows an ecliptic cut of a reconstructed picture of the solar wind density observed by STEREO HI. The Earth is the green dot, the Sun is in the center, seen from the solar north pole, and two SIRs resemble rotating sleeves. The intensity of grey corresponds to the normalized density value (darker means denser). The red circle indicates the SIR subsequently detected by ACE and STEREO A with a several day delay. For the corresponding movie see <http://helioweb.net>, click Archive – date - anim-sta1dej/anim-stb1dej.

A SIR represents a transition area from the slow to fast solar wind in which a compression, reflected in the enhanced N and B , is observed at the outer edge of a coronal hole flow, and V increases in its inner part. Therefore, SIRs may be imagined as dense turbulent shells surrounding high-speed rotating flows from coronal holes. The SIR is wider and more compressed at the leading and trailing edges of a coronal hole flow. At 1 AU, only a leading-edge SIR can easily be identified from in situ observations. Figure 2c shows that a typical feature characterizing an approach of the high-speed coronal hole flow is a growth of N in the background of a constant or slightly increasing V . After the passage of the stream interface (SI) at which N sharply falls but still remains above quiet period values and V sharply increases, the spacecraft occurs in the part of the SIR affected by the high-speed coronal hole flow in which V typically keeps growing. The SI located inside the SIR is a very bright and easy-to-identify structure that allows studying the SIR rotation via in situ observations successfully. In our case, we track the SI to compute the electric current density to check the location of CSs by an independent method (see 4. Validation).

The leading part of the SIR marked by yellow in Figure 2c has been used as a test bench to compute derivatives of B , β , and V_A/V (see 2.2 Method). In Figure 3 we show a typical example of the CS identification for the period of the ACE encounter with the SIR. Another example is the identification of CSs in a fragment of the same SIR observed by STEREO A (see Figure 4). Figure 4 is analogous to Figure 3. The threshold cutting off the noise is shown by the horizontal red line for each parameter. The spikes occurring out of the noise level indicate the CS location. The noise level is calculated as described in 2.2 Method. Only the spikes simultaneously observed in the B derivative and any of other parameters are treated as CS indicators.

As a result of the study, we have compiled a 1 AU CS list with the one second cadence for

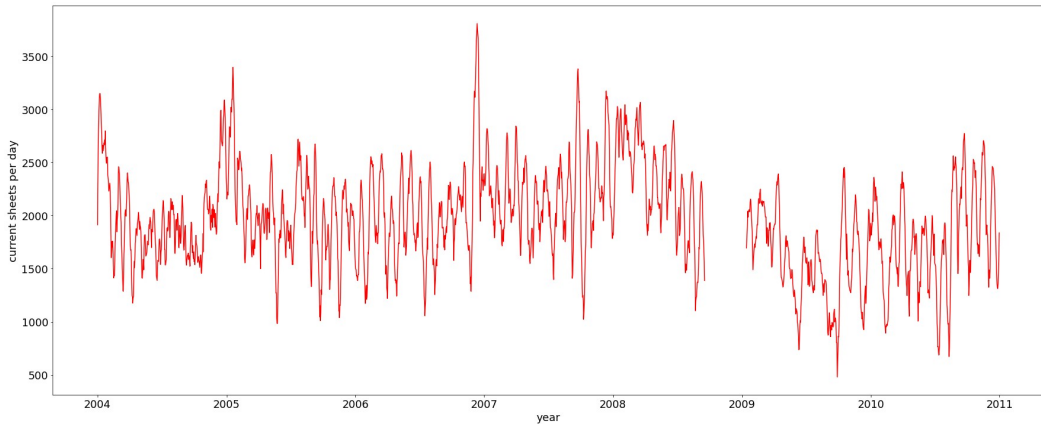


Figure 5. Number of CSs per day (R) observed at 1 AU. R is smoothed with a 27-day(point) Savitzky-Golay filter. The 3rd degree polynomial is used.

2004-2010. The CS database representing a set of the three-month-length CS lists is available at the dedicated IZMIRAN website <https://csdb.izmiran.ru>. The data description is provided at <https://csdb.izmiran.ru/data.html>. Additionally to indicating a location of each CS, the list contains the following parameters observed at the CS crossing: B , N , V , T , β , V_A , and three derivatives on the analysis of which the method is based (see 2.2 Method). This is an open access database, and the website does not require a registration, but a reference to the website and this article is necessary if one uses the CS database and/or the method.

3.2 What does determine the current sheet occurrence in the solar wind?

It is easy to find in Figure 3 and Figure 4 that the number of CSs may reach hundreds per hour or \sim several thousands per day in the most turbulent regions. Figure 5 illustrates this with a CS daily occurrence rate (R) observed in 2004-2010. The data are smoothed using a 27-point Savitzky-Golay filter with the 3rd degree polynomial (Savitzky & Golay, 1964). Based upon Figure 5, there is no obvious solar cycle dependence, although some decrease in the CS rate is observed in solar minimum. Further investigations will be made in this area when we extend the database.

The bright feature that meets the eye is quasi-regular variations seen in R . We find that this is a reflection of the CS production increase in turbulent and intermittent regions associated with SIRs/CIRs, the ICME sheaths and the related increase in the solar wind energy flow. A preliminary analysis allows us to conclude that the highest peaks of R seen in Figure 5 correspond to either SIR/CIR or ICME sheath observation periods. One can compare known ICME/SIR lists (see <http://www.srl.caltech.edu/ACE/ASC/DATA/level3/index.html>) with R to see this feature.

Here, we illustrate this point with Figure 6 that shows typical variations in R observed before, during and after a SIR (Figure 6a) and an ICME (Figure 6b). The SIR in Figure 6a was observed in the period of 3-5 May 2004. This is SIR no. 1 shown in Figure 3 of Jian et al., (2011). A shock pair did not form at the SIR’s edges at 1 AU at the SIR edge. Figure 6a shows that R quickly reaches its maximum within the SIR and slowly decreases afterwards within the

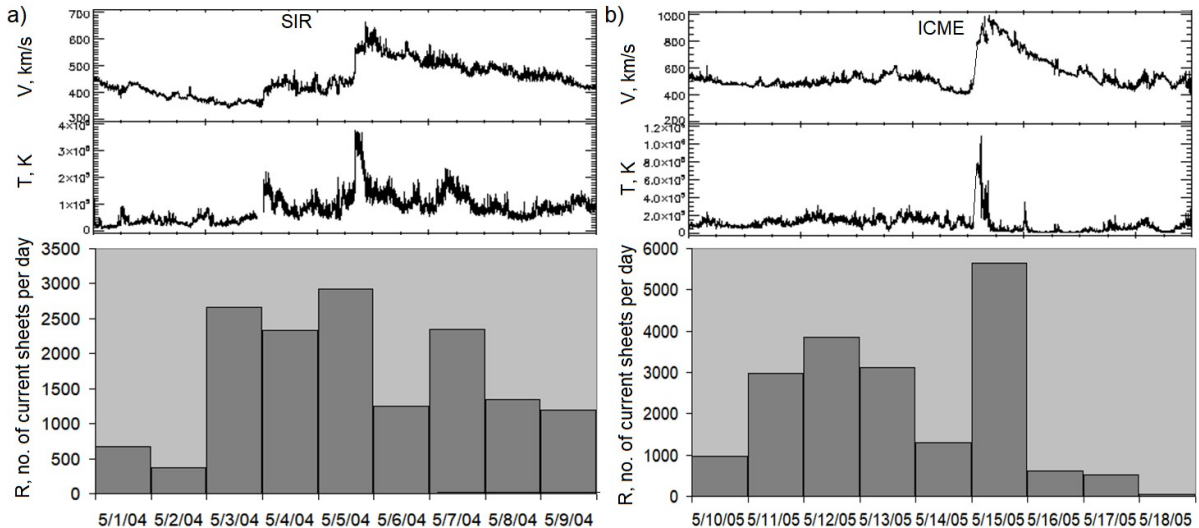


Figure 6. Typical variations of R associated with SIRs (a) and ICMEs (b). From top to bottom: solar wind speed V , temperature T , and R (from ACE).

associated coronal hole flow.

The very strong ICME detected by ACE from 15 May 2005 to 17 May 2005 was characterized by a classic ICME-driven forward interplanetary shock followed by the compressed turbulent sheath (see Figure 1 of Dasso et al., 2009) with which the R peak is associated (Figure 6b). An important feature seen in Figure 6b is a precursor representing a

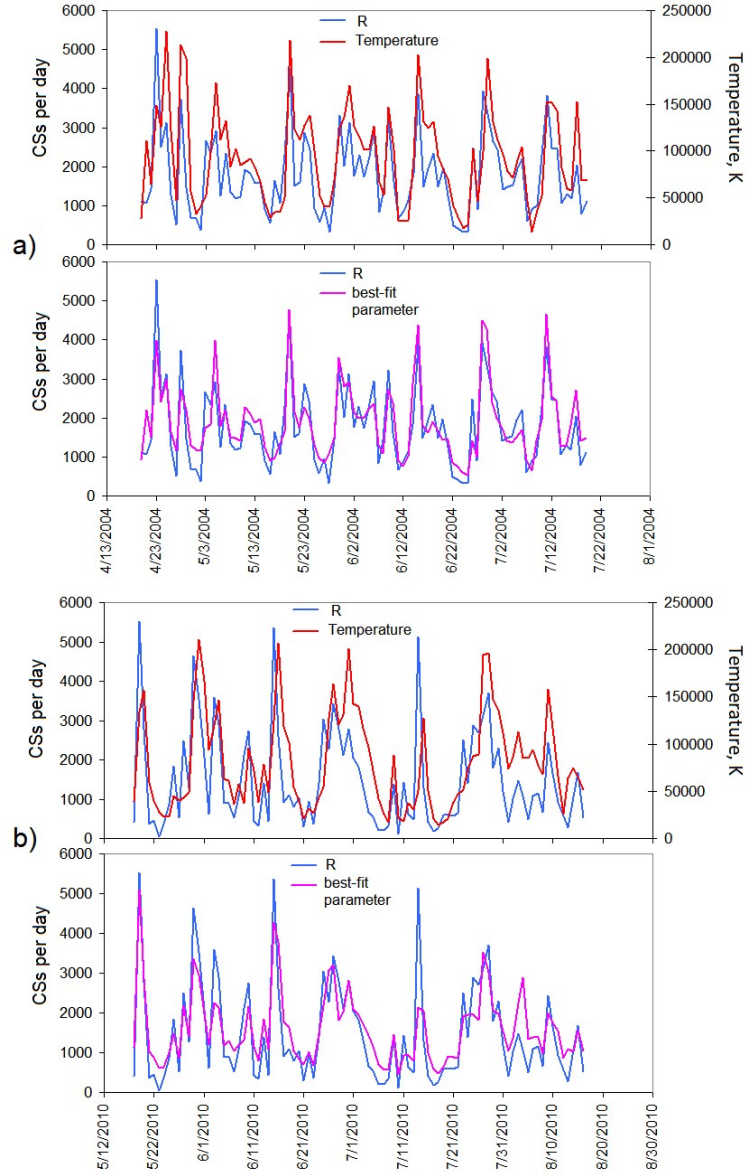


Figure 7. Finding the function that determines R . Examples are given for the three month-length periods in 2004 (a) and 2010 (b). Upper panels: the solar wind temperature T vs R . Lower panels: R vs the best-fit parameter $[V^2(N+5N') + 10T(N+N')]/5000$, where $N'=2\text{cm}^{-3}$ is the level of the background density of the undisturbed solar wind. Correlation coefficients between R and T (upper panels) are 0.72 (a) and 0.64 (b). Correlation coefficients between R and the best-fit parameter (lower panels) are 0.87 and 0.86, respectively. Based on the analysis of the data from ACE.

prolonged moderate R increase before the ICME approach. This phenomenon has been discussed before in terms of the crossing of a magnetic cavity filled with magnetic islands/plasmoids or flux ropes formed between the HCS and an ICME (Khabarova et al., 2016, 2017b, 2018; Adhikari et al., 2019). Note that the increase of the number of magnetic islands and the increase of the CS number are linked since magnetic islands are separated by CSs (e.g., Malandraki et al., 2019).

R correlates with T in a higher degree than with V and other key plasma/IMF parameters. The corresponding Pearson correlation coefficients C_{R-X} ($X=T, V, B, N$) calculated for the entire database from 2004 to 2010 are following: $C_{R-T}=0.66$, $C_{R-V}=0.46$, $C_{R-B}=0.43$, and $C_{R-N}=0.21$.

Let us derive a formula that expresses R as a function of physical parameters. CSs are characterized by an increased energy density compared to the surrounding plasma. In particular, CSs can be distinguished by the extrema of β and B because of that. Therefore, one can expect the number of CSs per day to be proportional to the average energy density in such regions. We will search for the best correlation between R and key solar wind parameters, trying to find a function (i.e., the best-fit parameter R_E) that depends on the kinetic energy density (the first term), the thermal energy density (the second term), and the magnetic field energy density (the third term).

$$R_E = \alpha_1 m_p V^2 (N + \alpha_2) / 2 + \alpha_3 (N + \alpha_4) k T + \alpha_5 B^2. \quad (1)$$

Here $\alpha_{1,2,3,4,5}$ are dimensional constant factors, m_p the proton mass, and k denotes the Boltzmann constant. V is measured in km/s, T - in K, N - in cm^{-3} , and B is measured in nT. Parameters α_1 , α_3 , and α_5 describe the impact of the corresponding types of energy on the CS rate, while α_2 and α_4 reflect the presence of the low-density plasma, in the background of which R_E variations caused by SIRs/CIRs and ICMEs occur.

An empirical search for the best-fit parameter shows that observed R highly correlates with a function of the following form:

$$R \sim (V^2 (N + N') + 10(N + N')T) / 5000 \quad (2)$$

Here, all values are reduced to the units of (1), and $N' = 2 \text{ cm}^{-3}$ corresponds to the concentration observed at 1 AU in the background solar wind. The magnetic field energy term is absent in (2) since its inclusion does not lead to obtaining a better result. The basis of a composite function method of the best correlation finding is described in Khabarova & Zastenker (2011) and Khabarova & Savin (2015).

Figure 7 shows examples of the comparison of R vs T and R vs the best-fit parameter in the form of (2) as observed for three months in 2004 (Figure 7a) and 2010 (Figure 7b). The correlation coefficient between R and the best-fit parameter is 0.82 for the whole 2004–2010 database. It may reach ~ 0.9 in some months. In particular, the correlation between R and the best-fit parameter is 0.87 in (Figure 7a) and 0.86 in (Figure 7b). This is far larger than any of correlation coefficients C_{R-X} ($X=T, V, B, N$) calculated for the same period.

One can find that (2) has the following general form in the CGS metric system:

$$R_E = (1.65 \cdot 10^{-2} (\rho + 5\rho') V^2 / 2 + 10(N + N') kT) / (5000 k \text{ cm}^{-3} \text{ K}). \quad (3)$$

Here $\rho = m_p N$ is the solar wind density, and $\rho' = m_p N'$. The denominator in (3) is a constant dimensional normalization factor. Meanwhile, observers will obtain R directly from the empirical formula (2), taking the parameters from the ACE database.

4 Validation of the method

4.1 Validation by the electric current density calculation

In order to check if the method of identifying CSs proposed above reflects reality in terms of revealing spatial variations of the electric current, we will estimate the current density \mathbf{j} and compare the location of its peaks with the location of CSs identified with our method.

To calculate \mathbf{j} in a chosen SIR/CIR's region, one should know details of the angular rotation of the SIR/CIR, which can be found if the SIR/CIR is subsequently detected by one spacecraft after another.

In the stationary case,

$$\text{rot} \mathbf{B} = \mu_0 \mathbf{j} , \quad (1)$$

here $\mu_0 = 1.256637062 \cdot 10^{-6}$ H/m in the SI system of units. The electric displacement currents can be ignored in the case of slowly evolving CSs. To have (1) in the form of the dependence of \mathbf{B} on coordinates, it is necessary to understand how a particular CIR/SIR moves. Here, we assume for simplicity that the only movement is CIR/SIR rotation around the rotation axis of the Sun in the [RT] plane with the angular velocity ω in the chosen reference Radial-Tangential-Normal frame (RTN). Then, $R = R_{AU} \cos(\omega t + \varphi)$ and $T = R_{AU} \sin(\omega t + \varphi)$, where φ is the initial phase, R_{AU} is the distance from the Sun to the spacecraft, which is different for each spacecraft involved in calculations.

Considering $\mathbf{B}(t)$ as $\mathbf{B}(t(R, T, N))$, where t is time, it is easy to find that

$$\mu_0 j_N = - \frac{dB_T}{dt} \frac{\sin(\omega t + \varphi)}{\omega R_{AU}} - \frac{dB_R}{dt} \frac{\cos(\omega t + \varphi)}{\omega R_{AU}} . \quad (2)$$

The initial phase φ can be chosen arbitrary. However, it determines whether the first and second terms are of the same order or not, which potentially may lead to the diminishing of the role of one of magnetic field components. Therefore, it is reasonable to take the following quantity j_0 to estimate the current density:

$$\mu_0 j_0 = - \frac{dB_T}{dt} \frac{1}{\omega R_{AU}} - \frac{dB_R}{dt} \frac{1}{\omega R_{AU}} \quad (3)$$

Here, j_0 is the upper limit for the electric current density in the N direction.

The next step is the calculation of the angular velocity. Let us introduce the following notations:

- Ω_L is the angular velocity of the spacecraft with respect to the Sun, where $L = 1, 2$ denotes, respectively, the 1st and the 2nd spacecraft that subsequently detect the rotating CIR/SIR front;
- Ω is the angular velocity of the CIR/SIR with respect to the Sun, determined by the difference t of the moments of arrival of the CIR/SIR front to the 1st (t_1) and 2nd spacecraft (t_2);
- $\text{HCI}_{L,1}$ is the heliographic longitude of the spacecraft L at t_1 in the Heliocentric Inertial (HCI) system of coordinates, and
- $\text{HCI}_{L,2}$ is the heliographic longitude of the spacecraft L at the point of time t_2 , in HCI.

Then the corresponding angular velocities are: $\Omega_1 = (\text{HCI}_{1,2} - \text{HCI}_{1,1}) / (t_2 - t_1)$; $\Omega_2 = (\text{HCI}_{2,2} - \text{HCI}_{2,1}) / (t_2 - t_1)$; $\Omega = (\text{HCI}_{2,2} - \text{HCI}_{1,1}) / (t_2 - t_1)$. The angular velocities of each spacecraft are different, so the angular velocity of the CIR/SIR relative to each spacecraft will be different. Therefore, $\omega = \Omega - \Omega_L$ is the angular velocity of the CIR/SIR with respect to the spacecraft L=1, 2.

The final step is the derivation of the formula for the electric current density. For the convenience of calculations, we transform (3) to the following form:

$$j_0 = -w (dB_T / dt + dB_R / dt) \quad (4),$$

where

$$w = \frac{1}{\mu_0 R_{AU} \omega} = \frac{10^4}{1.2566 \cdot 7 \cdot 215 \cdot [\omega] \cdot [R_{AU}]} \quad (5)$$

and $[\omega]$ is the angular velocity of the CIR/SIR with respect to the spacecraft under consideration, multiplied by 10^6 . $[R_{AU}]$ is the position of the spacecraft with respect to the Sun in astronomical

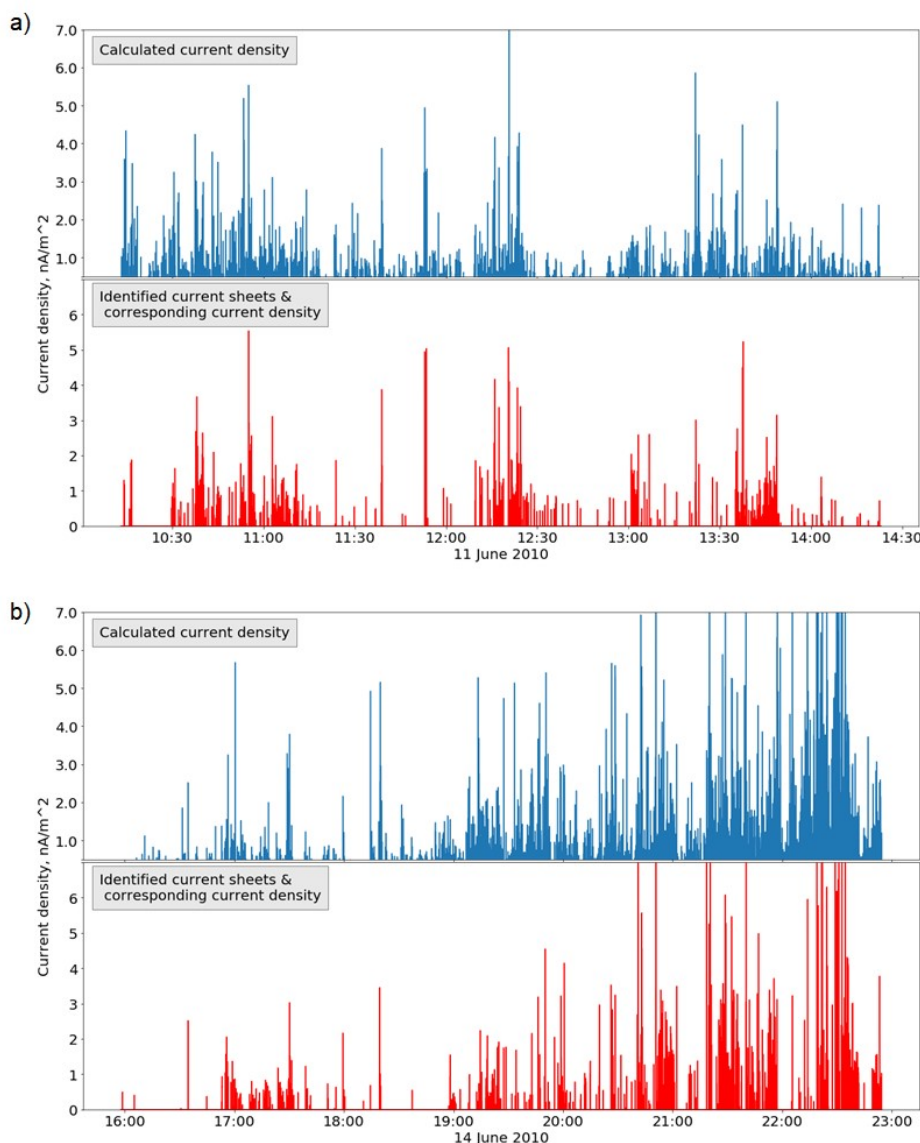


Figure 8. Electric current density calculated with an alternative method (top panels, blue bars) and CSs identified via the three-parameter method discussed above (bottom panels, red bars) for two randomly chosen time intervals of the event shown in Figure 2 by yellow stripe. Current density is cut off at 0.5 nA/m^2 to remove the noise. a) Example for the ACE spacecraft. b) Example for the STEREO A spacecraft.

units. If the magnetic field is measured in nT, then the current density will be in nA/m².

Note that since only sharp changes in the current density but not the absolute values matter for the analysis we propose, both $[\omega]$ and $[R_{AU}]$ can be considered as constants in SI for simplification. Meanwhile, other tasks would require detailed calculations of the parameters as described above. This technique can be considered as an additional and independent method of CS identification.

Figure 8a and Figure 8b represent a pair of two-panel graphs, the upper of which is for the electric current density and the lower depict the localization of CSs derived from the three-parameter method. For easier comparing, a typical “0-1” view of the CS location is modulated by the electric current density corresponding to each time at which a CS is identified (see the lower panels in Figure 8). Figure 8a shows calculations based on the ACE data, and Figure 8b shows the same for STEREO A. Fragments are arbitrary chosen from the “yellow stripe” region

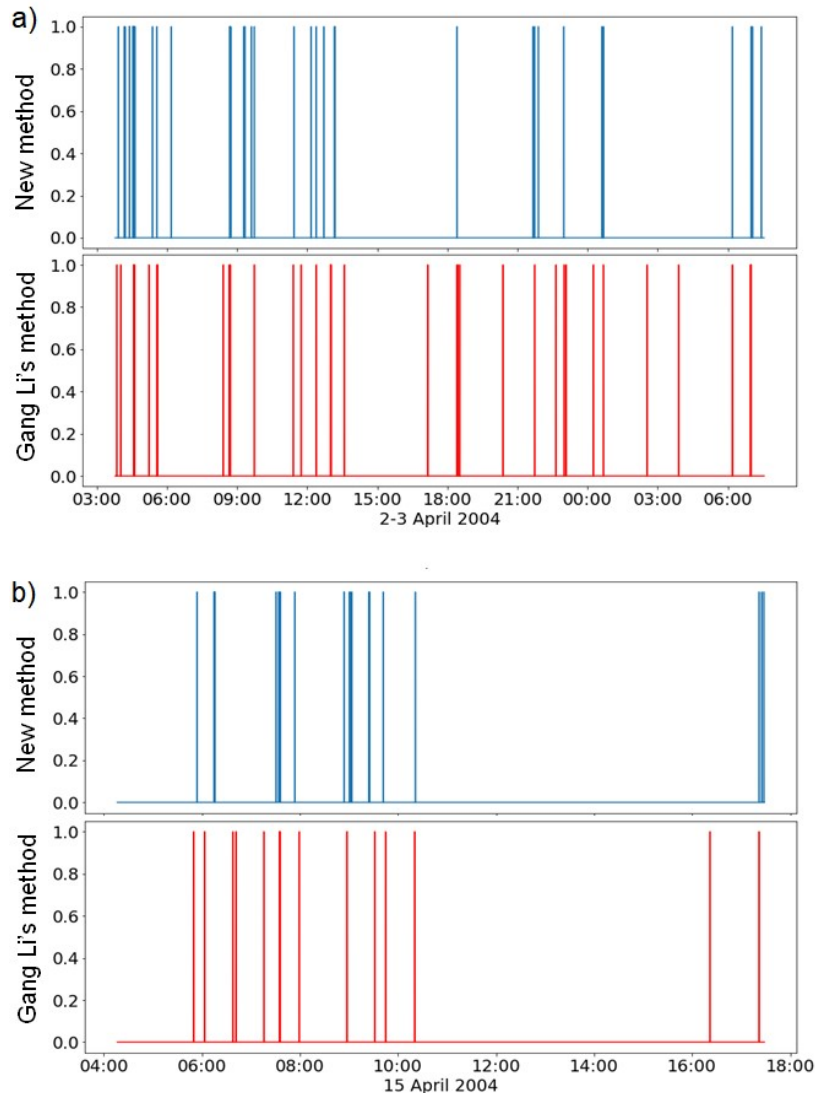


Figure 9. Comparison of results of the new three-parameter method (upper panels, blue bars) and Gang Li's method of CS identifying (lower panels, red bars). Randomly chosen time intervals on 2-3 April 2004 and 15 April 2004. Once second cadence. Based on the analysis of the ACE spacecraft data.

indicated in Figure 2. Comparing the location of spikes of the electric current density with the location of CSs from our CS database, one can conclude that the correlation between the two is very high, reaching 0.9.

4.2 Validation by the comparison with Gang Li’s method of CS identifying

Gang Li’s method (Li, 2008) is based on the analysis of local variations of the IMF direction that become dramatic at CSs. It is usually applied to identifying CSs in turbulent plasmas (see Introduction). On the one hand, we understand that the three-parameter method is completely different from (Li, 2008), but on the other hand, it would be useful to compare results of both.

We apply both techniques to the data obtained from the same spacecraft, ACE, in 2004. Figure 9a and Figure 9b show two fragments of the CS rows identified by our method (the upper panels) and Li’s method (the lower panels). The obtained results are promising. Despite the differences mentioned above, the correlation between the two rows is ~ 0.8 . The mismatches may be determined (i) by different targets of two methods (sometimes they identify not overlapping classes of CSs) and/or (ii) by different sensitivity of the methods because of the different cut off levels (see Introduction and Conclusions).

5 Discussion and Conclusions

A new method of the automated identification of current sheets has been created. We use an approach popular among observers to find CSs via a visual analysis of the behavior of both IMF and plasma parameters. The method suggests identifying CSs of various types, from short and unstable turbulence-born CSs embedded in the streaming solar wind to quasi-stable CSs associated with wave processes and large-scale solar-connected objects. A list of CSs identified at 1 AU from the 2004-2010 ACE data can be found at <https://csdb.izmiran.ru>.

The main statistical results preliminary obtained with the CS database are as following:

- On average, one-three thousands CSs are detected daily at the Earth’s orbit. A number of CSs per day is determined by the sum of the kinetic and thermal energy densities in a high degree (the 2004-2010 correlation coefficient is ~ 0.8).

The best-fit parameter is $(V^2(N+5N') + 10(N+N')T)/5000$ if V is given in km/s, T - in K, N is given in cm^{-3} , B is measured in nT, and $N'=2 \text{ cm}^{-3}$. The second, thermal term makes a one order larger input in the parameter than the kinetic one since the correlation with the temperature is better than with the speed. Meanwhile, without the first term, it is impossible to follow smaller-scale variations in the CS daily rate.

- The daily CS occurrence is found to be insensitive to the magnetic energy density variations.
- There is no obvious connection between the daily CS rate and the solar cycle. However, this preliminary conclusion should be reconsidered after the expansion of the CS database to several solar cycles.
- Peaks of the number of CSs per day are found to occur in SIRs/CIRs and ICME sheaths. The result is preliminary. We will provide a statistical report about this effect in the next publication.
- There is clustering of CSs. This fact is in agreement with the facts that (i) in realistic plasmas, the electric current is predicted to flow along multiple CSs rather than along one

(Kowal et al., 2012; Lazarian et al. 2020), (ii) multiple CSs with the electric current of the same direction tend to merge, and, on the other hand, (iii) strong CSs create an analogue of the plasma sheet consisting of secondary CSs around (e.g., Malova et al., 2017).

Understanding the physical nature of the obtained dependence between the CS occurrence and the solar wind energy density is a subject of future studies since it may be interpreted in different ways. On the one hand, a good correlation between the CS occurrence and the solar wind temperature has been known for years. It is often explained in terms of the solar wind heating by dissipation at turbulence-born CSs (e.g., Karimabadi et al., 2013; Wu et al., 2013; Wan et al., 2015, 2016; Adhikari et al., 2017). Meanwhile, the heating effect is supposed to be localized in the nearest vicinity of CSs, which is debated, especially for strong CSs. For example, Borovsky & Denton (2011) claim no correlation between strong CSs and local heating.

One can suggest from our results that CSs are intensively formed in hot plasma flows rather than represent a direct source of heating. Indeed, in addition to turbulence, CSs can appear at plasma irregularities caused by thermal fluctuations and asymmetries, which increase in regions with the raised temperature (Landau & Lifshitz, 1980, Lifshitz & Pitaevskii, 1981). CSs occur in such regions owing to the development of instabilities in plasma with temperature anisotropies and the increased magnetic reconnection rate (see Gingell et al., 2015 and references therein). Therefore, CSs may be formed due to local processes caused by large-scale plasma motions like those associated with SIRs/CIRs and ICMEs.

Substantial heating of particles can also be determined by intermittency, when the impact of turbulence-associated effects mentioned above is not essential. An intermittency phenomenon takes place if there are alternating regions with ordered laminar and turbulent flows (Landau and Lifshitz 1987, Landau et al., 1984). Regular quasi-stationary structures separated from chaotic regions by CSs are associated with such flows. In this case, the CSs can potentially gather in “sandwiches” consisting of several CSs due to the spatial quasi-periodicity (e.g., Bykov et al., 2008). This is consistent with the observed clustering of CSs. The sandwich-like regions may scatter some particles passing through those and accelerate other particles the phase of which turns out to be favorable upon entering the layer for example in the way suggested by Zelenyi et al. (2011).

The other aspect is that one may suggest that the good correlation between the CS occurrence rate and T is just because of the good T - V correlation (Borovsky & Denton, 2011). However, (i) the CS daily rate does not correlate with V well, and (ii) the good T - V correlation paradigm cannot be applied to SIRs and ICMEs in which R reaches its peak values, as seen from observations. Using an ICME as an example, Matthaeus et al. (2006) have shown that the correlation between V and T is significantly reduced in the presence of non-spherically-symmetric processes. One can see an illustration of this effect in Figure 6. T increases only for a short period at the leading edges of the fast speed coronal hole flow (Figure 6a) and the ICME (Figure 6b), but V remains high many hours after that. More studies are necessary to clarify this point.

Overall, many questions regarding properties of CSs in the solar wind and their impact on plasma heating and particle acceleration remain open. The CS list compiled as a result of this study opens an opportunity to answer the questions. The database will grow and include data for the entire period of 1 AU in situ observations starting with IMP8 and ending with the DSCOVR spacecraft. We also plan to compile CS lists for the STEREO spacecraft, Ulysses, Parker Solar

Probe and Solar Orbiter. The database is open access, and the community members are welcome to employ the method and the CS list for their statistical and case studies.

Acknowledgments and Data

We are grateful to the CDAWeb team for the for providing open access data for the magnetic field data from ACE (N. Ness, Bartol Research Institute) and the ACE/SWEPAM Solar Wind Experiment 64-second level 2 data (D.J. McComas, SWRI) at the CDAWeb platform <https://cdaweb.gsfc.nasa.gov>. The STEREO mission data are obtained from the UCLA STEREO Data Server (https://stereo-dev.epss.ucla.edu/l1_data) and CDAWeb (<https://cdaweb.gsfc.nasa.gov>). We thank Dusan Odstrcil for providing the solar wind density reconstructions from STEREO HI on the ENLIL Solar Wind Prediction website <http://helioweb.net>.

The database resulted from our study is available at <https://csdb.izmiran.ru>. The authors thank Andrei Osin for his help in maintaining the website at the IZMIRAN institutional server.

O.K. and R.K. are supported by Russian Science Foundation grant No. 20-42-04418. T.S. acknowledges the HSE’s general support and encouragement of student’s scientific activity.

References

Adhikari, L., G.P. Zank, P. Hunana, D. Shiota, R. Bruno, Q. Hu, and D. Telloni (2017), II. Transport of nearly incompressible magnetohydrodynamic turbulence from 1 to 75 au, *Astrophys. J.*, **841**, 85, aa6f5d, doi: 10.3847/1538-4357/aa6f5d

Azizabadi, A.C., N. Jain, and J. Büchner (2020), Identification and characterization of current sheets in collisionless plasma turbulence, arXiv:2009.03881, <https://arxiv.org/pdf/2009.03881>

Barnard, L., M.J. Owens, C.J. Scott, and C.A. de Koning (2020), Ensemble CME modeling constrained by heliospheric imager observations, *AGU Advances*, **1**, e2020AV000214. doi: 10.1029/2020AV000214

Behannon, K.W., F.M. Neubauer, and H. Barnstorff (1981), Fine scale characteristics of interplanetary sector boundaries. *J. Geophys. Res.*, **86**, 3273, doi: 10.1029/JA086iA05p03273

Bisi, M. M., B. V. Jackson, P. P. Hick, A. Buffington, D. Odstrcil, and J. M. Clover (2008), Three-dimensionalreconstructions of the early November 2004 Coordinated Data Analysis Workshop geomagnetic storms: Analyses of STELab IPSspeed and SMEI density data, *J. Geophys. Res.*, **113**, A00A11, doi:10.1029/2008JA013222

Blanco J.J., J. Rodriguez-Pacheco, M.A. Hidalgo, and J. Sequeiros (2006), Analysis of the heliospheric current sheet fine structure: Single or multiple current sheets, *J. Atm. Sol. Terr. Phys.*, **68**, 2173-2181, doi: 10.1016/j.jastp.2006.08.007

Borovsky, J. E., and M.H. Denton (2011), No evidence for heating of the solar wind at strong current sheets, *Astrophys. J. Lett.*, **739**, L61, <https://doi.org/10.1088/2041-8205/739/2/L61>

Borovsky, J. E., and B.L. Burkholder (2020), On the Fourier contribution of strong current sheets to the high-frequency magnetic power spectral density of the solar wind, *J. Geophys. Res.*, **125**, e2019JA027307, <https://doi.org/10.1029/2019JA027307>

Burkhart, B., S.M. Appel, S. Bialy, J. Cho, A.J. Christensen, D. Collins, C. Federrath, D.B. Fielding, D. Finkbeiner, and A.S. Hill (2020), *Astrophys. J.*, 905, abc484, doi : 10.3847/1538-4357/abc484

Bykov, A.A., L.M. Zelenyi and K.V. Malova (2008), Triple splitting of a thin current sheet: A new type of plasma equilibrium, *Plasma Phys. Rep.*, 34, 128–134, doi: 10.1134/S1063780X08020050

Conlon, T.M., S.E. Milan, J.A. Davies, and A.O. Williams (2015), Corotating Interaction Regions as Seen by the STEREO Heliospheric Imagers 2007–2010, *Sol. Phys.*, 290, 2291–2309, doi: 10.1007/s11207-015-0759-z

Dokken, T., T.R. Hagen, and J.M. Hjelmervik (2007), An Introduction to General-Purpose Computing on Programmable Graphics Hardware. In: Hasle G., Lie KA., Quak E. (eds) *Geometric Modelling, Numerical Simulation, and Optimization*. Springer, Berlin, Heidelberg, doi: 10.1007/978-3-540-68783-2_5

Eyles, C.J., Harrison, R.A., Davis, C.J. et al., (2009), The Heliospheric Imagers Onboard the STEREO Mission, *Sol. Phys.*, 254, 387–445, <https://doi.org/10.1007/s11207-008-9299-0>

Gingell, P.W., D. Burgess, and L. Matteini (2015), The three-dimensional evolution of ion-scale current sheets: tearing and drift-kink instabilities in the presence of proton temperature anisotropy, *Astrophys. J.*, 802, 4, doi: 10.1088/0004-637X/802/1/4

Gosling, J.T., R.M. Skoug, D.J. McComas, and C.W. Smith (2005), Direct evidence for magnetic reconnection in the solar wind near 1 AU, *J. Geophys. Res.*, 110, A01107, doi:10.1029/2004JA010809

Greco, A., W.H. Matthaeus, S. Perri, K.T. Osman, S. Servidio, M. Wan, and P. Dmitruk (2018), Partial Variance of Increments Method in Solar Wind Observations and Plasma Simulations, *Space Sci. Rev.*, 214, 1, doi: 10.1007/s11214-017-0435-8

Greco, A., W.H. Matthaeus, S. Servidio, P. Chuchai, and P. Dmitruk (2009), Statistical analysis of discontinuities in solar wind ace data and comparison with intermittent mhd turbulence, *Astrophys J.*, 691, L111, doi: 10.1088/0004-637X/691/2/L111

Hesse, M., M. Kuznetsova, and J. Birn (2001), Particle-in-cell simulations of three-dimensional collisionless magnetic reconnection, *J. Geophys. Res.*, 106, 29831-29841, doi: 10.1029/2001JA000075

Ho, C. M., B.T. Tsurutani, R. Sakurai, B.E. Goldstein, A. Balogh, and J.L. Phillips (1996), Interplanetary discontinuities in corotating streams and their interaction regions. *Astron. and Astrophys.*, 316, 346-349, <https://ui.adsabs.harvard.edu/#abs/1996A&A...316..346H/abstract>

Jackson, B.V., P.P. Hick, A. Buffington, M.M. Bisi, and J.M. Clover (2009), SMEI direct, 3-D-reconstruction sky maps, and volumetric analyses, and their comparison with SOHO and STEREO observations, 27, 4097–4104, *Ann. Geophys.*, doi: 10.5194/angeo-27-4097-2009

Jian, L., C.T. Russell, J.G. Luhmann, and R.M. Skoug (2006), Properties of Stream Interactions at One AU During 1995–2004, *Sol. Phys.*, 239, 337–392, doi: 10.1007/s11207-006-0132-3

Jian, L.K., C.T. Russell, J.G. Luhmann, P.J. MacNeice, D. Odstrcil, P. Riley, J.A. Linker, R M. Skoug, and J.T. Steinberg (2011), Comparison of Observations at ACE and Ulysses with Enlil Model Results: Stream Interaction Regions During Carrington Rotations 2016–2018, *Sol. Phys.*, 273, 179–203, doi: 10.1007/s11207-011-9858-7

Kaiser, M.L., T.A. Kucera, J.M. Davila, O.C.St. Cyr, M. Guhathakurta, and E. Christian (2008), The STEREO Mission: An Introduction, *Space Sci. Rev.* 136, 5–16, doi: 10.1007/s11214-007-9277-0

Khabarova, O., G.P. Zank, G. Li, J.A. le Roux, G.M. Webb, A. Dosch, and O.E. Malandraki (2015), Small-scale magnetic islands in the solar wind and their role in particle acceleration. 1. Dynamics of magnetic islands near the heliospheric current sheet, *Astrophys. J.*, 808, 181, doi: 10.1088/0004-637X/808/2/181

Khabarova, O., G.P. Zank, G. Li, O.E. Malandraki, J.A. le Roux, and G.M. Webb (2016), Small-scale magnetic islands in the solar wind and their role in particle acceleration. II. Particle energization inside magnetically confined cavities, *Astrophys. J.*, 827, 122, <https://doi.org/10.3847/0004-637X/827/2/122>

Khabarova O., V. Zharkova, Q. Xia, and O.E. Malandraki (2020), Counterstreaming strahls and heat flux dropouts as possible signatures of local particle acceleration in the solar wind, 894, L12, *Astrophys. J. Lett.*, <https://doi.org/10.3847/2041-8213/ab8cb8>

Khabarova, O.V., and G.P. Zank (2017), Energetic Particles of keV–MeV Energies Observed near Reconnecting Current Sheets at 1 au, *Astrophys. J.*, 843, 4, <https://doi.org/10.3847/1538-4357/aa7686>

Khabarova O.V., H.V. Malova, R.A. Kislov, L.M. Zelenyi, V.N. Obridko, A.F. Kharshiladze, M. Tokumaru, J.M. Sokół, S. Grzedzinski, and K. Fujiki (2017a), High-latitude conic current sheets in the solar wind, *Astrophys. J.*, 836, 108, <https://doi.org/10.3847/1538-4357/836/1/108>

Khabarova, O.V., G.P. Zank, O.E. Malandraki, G. Li, J.A. le Roux, and G.M. Webb (2017b), Observational Evidence for Local Particle Acceleration Associated with Magnetically Confined Magnetic Islands in the Heliosphere - a Review, *Sun and Geosp.*, 12, 23-30, <http://adsabs.harvard.edu/abs/2017SunGe..12...23K>

Khabarova O.V., O.E. Malandraki, G.P. Zank, G. Li, J.A. le Roux, and G.M. Webb (2018), Re-Acceleration of Energetic Particles in Large-Scale Heliospheric Magnetic Cavities, *Proc. of the International Astronomical Union, Symposium S335: Space Weather of the Heliosphere: Processes and Forecasts*, July 2017, 13, 75-81, doi: 10.1017/S1743921318000285

Khabarova, O., and G. Zastenker (2011), Sharp changes in solar wind ion flux and density within and out of current sheets, *Sol. Phys.*, 270, 311-329, DOI: 10.1007/s11207-011-9719-4

Khabarova, O., and I. Savin (2015), Changes in Environmental Parameters and Their Impact on Forest Growth in Northern Eurasia, *Atmosph. and Climate Sci.*, 5, 91-105, doi: 10.4236/acs.2015.52007

Kislov, R.A., O. Khabarova, and H.V. Malova (2015), A new stationary analytical model of the heliospheric current sheet and the plasma sheet, 120, 8210-8228, *J. Geophys. Res.*, <https://doi.org/10.1002/2015JA021294>

Kislov, R.A., O.V. Khabarova, and H.V. Malova (2019), Quasi-stationary Current Sheets of the Solar Origin in the Heliosphere, *Astrophys. J.*, 875, 28, <https://doi.org/10.3847/1538-4357/ab0dff>

Kowal, G., A. Lazarian, E.T. Vishniac, and K. Otmianowska-Mazur (2012), Reconnection studies under different types of turbulence driving, *Nonlin. Processes Geophys.*, 19, 297–314, <https://doi.org/10.5194/npg-19-297-2012>

Landau, L. D., & Lifshitz, E. M. (1980). Fluctuations. In L. D. Landau, E. M. Lifshitz (eds.), *Statistical physics (Third edition), Course of theoretical physics* (Vol. 5, pp. 333-400), Oxford: Butterworth-Heinemann, doi: 10.1016/B978-0-08-057046-4.50019-1

Landau, L. D., & Lifshitz, E. M. (1987). Turbulence. In L. D. Landau, E. M. Lifshitz (eds.), *Fluid mechanics (Second edition), Course of theoretical physics* (Vol. 6, pp. 95-156), Oxford: Butterworth-Heinemann, doi: 10.1016/B978-0-08-033933-7.50011-8

Landau, L. D., Lifshitz, E. M., & Pitaevskii, L. P. (1984). Magnetohydrodynamics. In L. D. Landau, E. M. Lifshitz (eds.), *Electrodynamics of continuous media (Second edition), Course of theoretical physics* (Vol. 8, pp. 225-256), Oxford: Butterworth-Heinemann

Lazarian, A., G.L. Eyink, A. Jafari, G. Kowal, H. Li, S. Xu , and E.T. Vishniac (2020), 3D turbulent reconnection: Theory, tests, and astrophysical implications, *Phys. Plasmas*, 27, 012305, doi: 10.1063/1.5110603

le Roux, J. A., Zank, G. P., & Khabarova, O. V. (2018) Self-consistent Energetic Particle Acceleration by Contracting and Reconnecting Small-scale Flux Ropes: The Governing Equations, *Astrophys. J.*, 864, 158, doi: 10.3847/1538-4357/aad8b3

Le Roux, J. A., Webb G.M., Khabarova O.V., Zhao L.-L., and Adhikari L. (2019), Modeling Energetic Particle Acceleration and Transport in a Solar Wind Region with Contracting and Reconnecting Small-scale Flux Ropes at Earth Orbit, *Astrophys. J.*, 887, 77, doi: 10.3847/1538-4357/ab521f

le Roux J.A., G.M. Webb, O.V. Khabarova, K.T. Van Eck, L.-L. Zhao, L. Adhikari, Journal of Physics: Conference Series (19th Annual International Astrophysics Conference 9-13 March 2020 in Santa Fe, New Mexico, USA) (2020), 1620, 012008, doi:10.1088/1742-6596/1620/1/012008, <https://iopscience.iop.org/article/10.1088/1742-6596/1620/1/012008>

Lifshitz, E. M., & Pitaevskii, L. P. (1981). Collisions in plasmas. In E. M. Lifshitz, L. P. Pitaevskii (eds.), *Physical kinetics (First edition), Course of theoretical physics* (Vol. 10, pp. 168-216), Oxford: Butterworth-Heinemann, doi: 10.1016/B978-0-08-057049-5.50009-6

Maiewski, E.V., H.V. Malova, R.A. Kislov, V.Yu. Popov, A.A. Petrukovich, O.V. Khabarova, and L.M. Zelenyi (2020), Formation of Multiple Current Sheets in the Heliospheric Plasma Sheet, *Cosmic Res.*, 58, 411–425, doi: 10.1134/S0010952520060076

Malandraki, O., O. Khabarova, R. Bruno, G.P. Zank, G. Li, B. Jackson, M.M. Bisi, A. Greco, O. Pezzi, W. Matthaeus, A.G. Chasapis, S. Servidio, H. Malova, R. Kislov, F. Effenberger, J. le Roux, Y. Chen, Q. Hu, and E. Engelbrecht (2019), Current sheets, magnetic islands and associated particle acceleration in the solar wind as observed by Ulysses near the ecliptic plane, *Astrophys. J.*, 881, 116, doi: 10.3847/1538-4357/ab289a

Malova, Kh.V., V.Yu. Popov, O.V. Khabarova, E.E. Grigorenko, A.A. Petrukovich, and L.M. Zelenyi (2018), Structure of Current Sheets with Quasi-Adiabatic Dynamics of Particles in the Solar Wind, *Cosmic Res.*, 56, 462–470, doi: 10.1134/S0010952518060060

Matthaeus, W.H., H.A. Elliott, and D.J. McComas (2006), Correlation of speed and temperature in the solar wind, *J. Geophys. Res.*, 111, A10103, doi:10.1029/2006JA011636

Mingalev, O.V., I.V. Mingalev, H.V. Malova, A.M. Merzlyi, V.S. Mingalev, and O.V. Khabarova (2020), Description of Large-Scale Processes in the Near-Earth Space Plasma, *Plasma Phys. Rep.*, 46, 374–395, doi: 10.1134/S1063780X20030083

Mingalev, O.V., O.V. Khabarova, H.V. Malova, I.V. Mingalev, R.A. Kislov, M.N. Mel’nik, P.V. Setsko, L.M. Zelenyi, and G.P. Zank, *Sol. Syst. Res.* (2019) doi: 10.1134/S0038094619010064

Muñoz, P.A., and Büchner, J. (2018), Kinetic turbulence in fast three-dimensional collisionless guide-field magnetic reconnection, *Phys. Rev. E*, 98, doi:10.1103/physreve.98.043205

Pecora, F., S. Servidio, A. Greco, and W.H. Matthaeus (2021), Identification of coherent structures in space plasmas: The magnetic helicity-PVI method, *Astron. and Astrophys.*, doi: 10.1051/0004-6361/202039639

Phan, T.D., S.D. Bale, J.P. Eastwood, et al., (2020), Parker Solar Probe In Situ Observations of Magnetic Reconnection Exhausts during Encounter 1. *Astrophys. J. Suppl. Ser.*, 246, 34, doi:10.3847/1538-4365/ab55ee

Podesta, J. J. (2017), The most intense current sheets in the high-speed solar wind near 1 AU, *J. Geophys. Res.*, 122, 2795–2823, doi:10.1002/2016JA023629

Pritchett P.L. (2003) Particle-in-Cell Simulation of Plasmas— A Tutorial. In: Büchner J., Scholer M., Dum C.T. (eds) *Space Plasma Simulation. Lecture Notes in Physics*, 615, Springer, Berlin, Heidelberg, https://doi.org/10.1007/3-540-36530-3_1

Richardson, I.G. (2018), Solar wind stream interaction regions throughout the heliosphere. *Living Rev. in Solar Phys.*, 15, 1, doi:10.1007/s41116-017-0011-z

Rouillard, A.P., J.A. Davies, R.J. Forsyth, et al., (2008), First imaging of corotating interaction regions using the STEREO spacecraft, *Geophys. Res. Lett.*, 35, L10110, doi: 10.1029/2008GL033767

Savitzky, A., and M.J.E. Golay (1964), Smoothing and Differentiation of Data by Simplified Least Squares Procedures, *Analytical Chemistry*, 36, 1627-1639, doi: 10.1021/ac60214a047

Scott, C.J., M.J. Owens, C.A. de Koning, L.A. Barnard, S.R. Jones, and J. Wilkinson (2019), Using ghost fronts within STEREO Heliospheric Imager data to infer the evolution in longitudinal structure of a coronal mass ejection, *Space Weather*, 17, 539–552, doi: 10.1029/2018SW002093

Simunac, K.D.C., A.B. Galvin, C.J. Farrugia, et al., (2012), The Heliospheric Plasma Sheet Observed in situ by Three Spacecraft over Four Solar Rotations, *Solar Phys.*, 281, 423-447, doi: 10.1007/s11207-012-0156-9

Stantchev, G., D. Juba, W. Dorland, and A. Varshney (2009), Using Graphics Processors for High-Performance Computation and Visualization of Plasma Turbulence, *Computing in Sci. and Engineering*, 11, 52-59, doi: 10.1109/MCSE.2009.42

Stone, E.C., A.M. Frandsen, R.A. Mewaldt, E.R. Christian, D. Margolies, J.F. Ormes, and F. Snow (1998), The Advanced Composition Explorer, *Space Sci. Rev.*, 86, 1–22, doi: 10.1023/A:1005082526237

Suess, S.T., Y.-K. Ko, R. von Steiger, and R.L. Moore (2009), Quiescent current sheets in the solar wind and origins of slow wind, *J. Geophys. Res.*, 114, A04103, doi: 10.1029/2008JA013704

Tan, L.C. (2020), An Alternative Interpretation of Impulsive SEP Events Occurring on 1999 January 9–10, *Astrophys. J.*, 901, 120, doi: 10.3847/1538-4357/abb086

Tessein, J. A., C.W. Smith, B.J. Vasquez, and R.M. Skoug (2011), Turbulence associated with corotating interaction regions at 1 AU: Inertial and dissipation range magnetic field spectra, *J. Geophys. Res.*, 116, A10104, doi:10.1029/2011JA016647

Wan, M., W.H. Matthaeus, V. Roytershteyn, T.N. Parashar, P. Wu, and H. Karimabadi (2016), Intermittency, coherent structures and dissipation in plasma turbulence, *Phys. of Plasmas*, 23, 042307, doi: 10.1063/1.4945631

Wan, M., W. H. Matthaeus, V. Roytershteyn, H. Karimabadi, Parashar T. , Wu P. , and Shay M. (2015), Intermittent Dissipation and Heating in 3D Kinetic Plasma Turbulence, *Phys. Rev. Lett.*, 114, 175002, doi: 10.1103/PhysRevLett.114.175002

Wu, P.; Perri S., Osman K., M. Wan, W.H. Matthaeus, M.A. Shay, M.L. Goldstein, H. Karimabadi, and S. Chapman (2013), Intermittent Heating in Solar Wind and Kinetic Simulations, *Astrophys. J. Lett.*, 763, L30, doi: 10.1088/2041-8205/763/2/L30

Xia, Q., & V. Zharkova (2018), Particle acceleration in coalescent and squashed magnetic islands. I. Test particle approach, *Astron. Astrophys.*, 620, A121, doi: 10.1051/0004-6361/201833599

Xia, Q., & V. Zharkova (2020), Particle acceleration in coalescent and squashed magnetic islands. II. Particle-in-cell approach, *Astron. Astrophys.*, 635, A116, doi: 10.1051/0004-6361/201936420

Zelenyi, L.M., H.V. Malova, E.E. Grigorenko, and V.Y. Popov (2016), Thin current sheets: from the work of Ginzburg and Syrovatskii to the present day, *Physics-Uspekhi*, 59, 1057–1090, doi:10.3367/ufne.2016.09.037923

Zelenyi, L.M., H.V. Malova, E.E. Grigorenko, V.Y. Popov, and E.M. Dubinin (2020), Universal scaling of thin current sheets, *Geophys. Res. Lett.*, 47, e2020GL088422, 1-10, doi: 10.1029/2020GL088422

Zelenyi, L.M., S.D. Rybalko, A.V. Artemyev, A.A. Petrukovich, and G. Zimbardo (2011), Charged particle acceleration by intermittent electromagnetic turbulence, *Geophys. Res. Lett.*, 38, L17110, doi:10.1029/2011GL048983

Zhang, T.L., C.T. Russell, W. Zambelli, Z. Vörös, C. Wang, J.B. Cao, L.K. Jian, R. J. Strangeway, M. Balikhin, W. Baumjohann, M. Delva, M. Volwerk, and K.-H. Glassmeier (2008), Behavior of current sheets at directional magnetic discontinuities in the solar wind at 0.72 AU, *Geophys. Res. Lett.*, 35, L24102, doi: 10.1029/2008GL036120

Zhdankin, V., D.A. Uzdensky, J.C. Perez, and S. Boldyrev (2013), Statistical analysis of current sheets in three-dimensional magnetohydrodynamic turbulence, *Astrophys. J.*, 771, 124, doi: 10.1088/0004-637X/771/2/124